JASET KMUTNB
Research Article

Journal of Applied Science and Emerging Technology (JASET)
Published by Faculty of Applied Science, KMUTNB, Thailand
doi: 10.14416/JASET.KMUTNB.2025.03.002
Vol. 24, No. 3 [2025]: e264720

Thermodynamic Modeling of Experimental Data for the Adsorption of Ternary Antibiotic Mixture from Aqueous Solution Using Flamboyant-Pod-Based Activated Carbon

Ojo Ilesanmi Ademola[1,2]*, Ajani Adegbenro Sunday[1], Ajani Oluwatayo Sandra[3], and Mustapha Lateef Olajuwon[2]

[1]Department of Physics and Material Science, Faculty of Pure and Applied Sciences, Kwara State University, Malete, Nigeria.
[2]Department of Physical Sciences, Faculty of Natural and Applied Sciences, Al-Hikmah University, Ilorin, Kwara State, Nigeria.
[3]Department of Medicine, Ladoke Akintola University of Technology Teaching Hospital, P.M.B 4001, Ogbomoso, Oyo state, Nigeria.

* Corresponding Author, E-mail: iaojo@alhikmah.edu.ng DOI: 10.14416/JASET.KMUTNB.2025.03.002
Received 6 November 2025; **Revised** 19 December 2025; **Accepted** 25 December 2025

ABSTRACT

Antibiotic contamination in water poses significant environmental and public health risks, necessitating low-cost and sustainable treatment solutions. This study explores the development of Flamboyant-Pod-based Activated Carbon (FPAC), a bio-based adsorbent, for the removal of a Ternary Antibiotic Mixture (TAM). Raw Flamboyant Pods (FPs) were pretreated, chemically activated with Potassium Hydroxide (KOH), and carbonized at 500 °C for 40 min. The structural and surface modifications of FPAC were characterized using Scanning Electron Microscopy (SEM), Energy-Dispersive X-ray (EDX) analysis and Fourier Transform Infrared Spectroscopy (FTIR) analysis. Batch adsorption experiments were performed under varying conditions of contact time (10-240 min), initial concentrations (20-100 mg/L), and temperatures (40-60 °C). Adsorption thermodynamic parameters, including Gibb's Free Energy (ΔG°), Enthalpy Change (ΔH°), Entropy Change (ΔS°), Isosteric Heat of Adsorption (ΔH_x), Activation Energy (E_a), Sorption Probability (S*), Surface Coverage (θ), and Hopping Number (n), were evaluated to determine adsorption feasibility and mechanisms. FPAC exhibited a porous structure with enhanced carbon content and new functional groups, promoting chemical interactions with antibiotics. Adsorption proceeded rapidly within the first 100 min, achieving maximum capacities of 9.371 mg/g (Amoxicillin, AMO), 9.310 mg/g (Tetracycline, TETRA), and 8.733 mg/g (Ampicillin, AMP). Corresponding removal efficiencies were 85.91, 91.24, and 78.67%. Thermodynamic analysis revealed negative ΔG° and ΔH° values, confirming a spontaneous and exothermic process, while ΔH_x and E_a values indicated predominantly physisorption-driven adsorption. The findings establish FPAC as an efficient, low-cost, and environmentally friendly adsorbent with strong potential for the remediation of antibiotic-contaminated wastewater.

KEYWORDS: Activated carbon, Flamboyant pod, Antibiotic, Adsorption, Thermodynamic

Please cite this article as: A. Ojo S. Ajani S. Ajani and O. Mustapha, "Thermodynamic Modeling of Experimental Data for the Adsorption of Ternary Antibiotic Mixture from Aqueous Solution Using Flamboyant-Pod-Based Activated Carbon," *Journal of Applied Science and Emerging Technology,* vol 24, no 3, pp. 1-13, ID. 264720, December 2025

1. INTRODUCTION

Water pollution, particularly from industrial and pharmaceutical waste, is a major global environmental challenge (Dufatanye et al., 2022; Gautam et al., 2024). Untreated wastewater discharged into natural water bodies degrades ecosystems, threatens biodiversity, and contributes to the spread of waterborne diseases (Abdelkarim and Djamila, 2020; Ortúzar et al., 2022). Among the pollutants of growing concern are pharmaceutical residues, especially antibiotics, which persist in aquatic environments and contribute to the development of antibiotic-resistant bacteria (Nomngongo and Chaba, 2019; Azarpira et al., 2019). Conventional wastewater treatment methods such as coagulation, flocculation, membrane separation, and chemical oxidation are often costly, inefficient, and produce toxic sludge (Renugadevi and Krishnaveni, 2021). Adsorption, in contrast, is widely regarded as a superior method due to its low cost, efficiency, ease of operation, and ability to remove diverse pollutants (Azarpira et al., 2019). However, the search for inexpensive, renewable, and effective adsorbents remains critical.

Flamboyant pod (Delonix regia) is an abundant agricultural residue that contributes to solid waste disposal problems in tropical regions (Abulude and Adejayan, 2017). Converting flamboyant pods waste into activated carbon provides a sustainable strategy for both waste management and water purification. Previous studies have demonstrated that activation with alkaline agents, such as KOH, enhances pore development and surface functionality, improving adsorption capacity (Ravichandran et al., 2018; Deyi et al., 2023).

Tetracyclines have been widely applied not only in human and veterinary medicine but also at sub-therapeutic levels in animal feed as growth promoters due to their low cost and broad antimicrobial activity (Fomnya et al., 2021). They are among the most frequently detected antibiotics in the environment, ranking second globally in occurrence. Studies have revealed that tetracyclines are harmful to aquatic organisms. They inhibit the growth of various algal species and display embryotoxic effects in fish, highlighting their potential to disrupt aquatic ecosystems (Roberts and Chopra, 2021). The environmental persistence and biological impacts of tetracyclines underscore the urgent need for effective wastewater treatment strategies to mitigate their release and accumulation. The chemical structure of tetracycline is shown in Scheme 1.

Amoxicillin is also the most commonly prescribed antibiotic for children and for the treatment of bacterial infections. Over 80% of orally administered amoxicillin in humans is excreted unchanged in urine within two hours of consumption (Barbooti and Zahraw, 2020). Traces of the drug and its degradation products are frequently detected in aquatic environments. The predominant environmental sources of amoxicillin include the excretion of unmetabolized antibiotics by humans and animals, the disposal of unused or expired drugs, and wastewater discharges from pharmaceutical manufacturing plants (Choffor-Nchinda et al., 2018). The chemical structure of amoxicillin is shown in Scheme 2.

Ampicillin is used to treat a variety of bacterial infections, including ear and respiratory tract infections, and endocarditis. In obstetrics, it is used for the prevention of group B streptococcal infections in newborns and for in utero therapy. It also has applications in veterinary medicine, for example, in the treatment of *Clostridium* infections in poultry (Nafisur and Poornima, 2020). Ampicillin is regarded as a non-biodegradable antibiotic due to its persistence in the environment, and its removal has

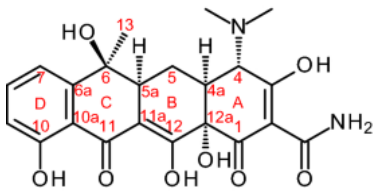

Scheme 1 Chemical structure of tetracycline (Roberts and Chopra, 2021)

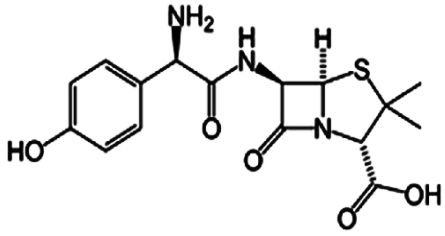

Scheme 2 Chemical structure of amoxicillin (Barbooti and Zahraw, 2020)

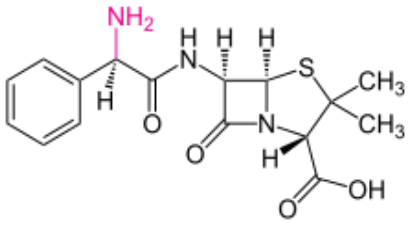

Scheme 3 Chemical structure of ampicillin (Nafisur and Poornima, 2020)

become an important focus in environmental remediation studies. The chemical structure of ampicillin is shown in Scheme 3.

Most adsorption studies focus on single-solute systems, yet real wastewater typically contains multicomponent mixtures (Wei et al., 2019; Alnajrani and Alsager, 2020; Amrutha et al., 2023). Investigating adsorption in multicomponent systems is therefore essential for real-world applications. This study develops activated carbon from flamboyant pods and applies it for the adsorption of a ternary antibiotic mixture (tetracycline, ampicillin, and amoxicillin) from aqueous solutions. The research integrates thermodynamic analyses to understand the adsorption mechanism and establish the feasibility of FPAC as a low-cost, eco-friendly adsorbent for pharmaceutical wastewater remediation.

2. MATERIALS AND METHODS

2.1 Equipment, Chemicals and Sample

The experimental setup included a muffle furnace, mechanical flask shaker, digital analytical balance, UV-Vis spectrophotometer, rotary shaker, magnetic stirrer, pH meter, thermometer, desiccator, oven, Fourier transform infrared spectroscopy (FTIR, Varian 660 MidIR Dual MCT/DTGS Bundle with ATR) and Scanning electron microscopy (SEM, Hitachi SU 3500, Tokyo, Japan).

Selected antibiotics (AMO, TETRA, and AMP) were purchased from One Step Pharmaceutical Store, Ilorin. Analytical-grade chemicals and reagents used include potassium hydroxide, hydrochloric acid, sodium hydroxide, potassium bromide, potassium sulphate, barium chloride, sulphuric acid, and phenanthroline. All were used as received without further purification.

2.2 Sample Pre-treatment

Flamboyant pods were collected from Mandate Estate, Ilorin, Nigeria (8.4752 °N, 4.5058 °E). The pods were washed, rinsed with distilled water, cut into smaller pieces, sun-dried, ground, and sieved (425-850 μm) using a sieve shaker (Deyi et al., 2023).

2.3 Activation and Carbonization of FPAC

Potassium hydroxide solutions of different molarities (0.5, 0.75, and 1.0 M) were prepared by dissolving 28, 42, and 56 g of KOH, respectively, in 1 L of distilled water. Equal particle sizes of FP (10 g) were then soaked in 100 mL of KOH solution (0.5-1.0 M) at room temperature for 24 h. After soaking, the mixture was evaporated to a paste, cooled, thoroughly washed with distilled water, and neutralized using 0.1 M HCl and 0.1 M NaOH until the pH reached 6.9-7.1. The resulting material was oven-dried at 105 °C overnight, cooled in a desiccator, and subsequently carbonized in a muffle furnace at 500 °C for 40 min (Ravichandran et al., 2018; Nomngongo and Chaba, 2019).

2.4 Characterization of FPAC

Surface chemistry was analyzed by mixing FP samples with potassium bromide in a 1:100 ratio. Spectra were recorded in the 4000-400 cm^{-1} range at 4 cm^{-1} resolution with 200 scans per sample (George et al., 2014; Mashkovtsev et al., 2023). Morphological features of FPAC were examined using SEM after sputter-coating with a 20 nm gold layer. Images were recorded at variable magnifications to study pore development (Ravichandran et al., 2018; Sarwar et al., 2021).

2.5 Optimization of TAM Stock Solutions

The TAM mixing ratio was developed using an I-Optimal Coordinate Exchange Design Model (IOCEDM) of Design Expert software. The aggregate concentration (100 mg/L) of the AMO, TETRA and AMP mixture was dissolved in distilled water at the different mixing ratios suggested by IOCEDM. Absorbance was recorded at maximum wavelength (λ_{max}) of 286.56 nm (AMO), 361.17 nm (TETRA), and 288.37 nm (AMP) with a UV-Vis spectrophotometer. Calibration curves of absorbance against concentration were developed for quantitative analysis (Okoye et al., 2018).

2.6 Batch Adsorption Experiments

Initial concentrations of 20-100 mg/L, contact time from 10 to 240 min and the effect of temperaure at 40-60 °C were tested using 1.0 g of FPAC in 100 mL TAM solution. Samples were shaken at 180 rpm at room temperature and neutral pH. Supernatant was centrifuged at 180 rpm for 20 min before UV-Vis analysis (Hasan et al., 2014; Rahmanian et al., 2018; Deyi et al., 2023). The Adsorption Capacity (q_e, mg/g) and Removal Efficiency (R_e, %) were calculated using Equations 2.1 and 2.2.

$$q_e = \frac{V(C_o - C_e)}{W} \quad (2.1)$$

$$R_e = \frac{(C_o - C_e)}{C_o} \times 100\% \quad (2.2)$$

where V is the solution volume (L), C_o and C_e are initial and equilibrium concentrations (mg/L), and W is adsorbent weight (g).

2.7 Thermodynamic Parameters

The thermodynamic properties of the selected TAM adsorption onto the FPAC developed were investigated based on the existing adsorption thermodynamics models. These properties often give insight into the nature (physisorption or chemisorption) and the impact of the temperature-prompted energy of the adsorption process (Sahmoune, 2018; Zeng et al., 2024).

2.7.1 Gibb's free energy, enthalpy change and entropy change

Gibb's free energy, enthalpy change and entropy change of the adsorption study were investigated based on Equations 2.3-2.6. The values of $\Delta H°$ and $\Delta S°$ are evaluated from the slope and intercepts of the linear plot of $\ln K_c$ against $\frac{1}{T}$ (Batool et al., 2018; Korkmaz and Tuna, 2025).

$$k_c = \frac{C_0 - C_e}{C_e} \quad (2.3)$$

$$\Delta G^0 = -RT\ln K_c \quad (2.4)$$

$$\Delta G^0 = \Delta H - T\Delta S \quad (2.5)$$

$$\ln k_c = \frac{\Delta S}{R} - \frac{\Delta H}{RT} \quad (2.6)$$

2.7.2 Isosteric heat of adsorption

The Isosteric heat of adsorption constants, ΔH_x and K were determined from the slope and intercept, respectively from the plot of $\ln C_e$ against $\frac{1}{T}$ from Equations 2.7 and 2.8 (Patil et al., 2024)

$$\frac{d \ln C_e}{dT} = \frac{-\Delta H_x}{RT^2} \quad (2.7)$$

$$\ln C_e = -\frac{\Delta H_x}{R}\frac{1}{T} + K \quad (2.8)$$

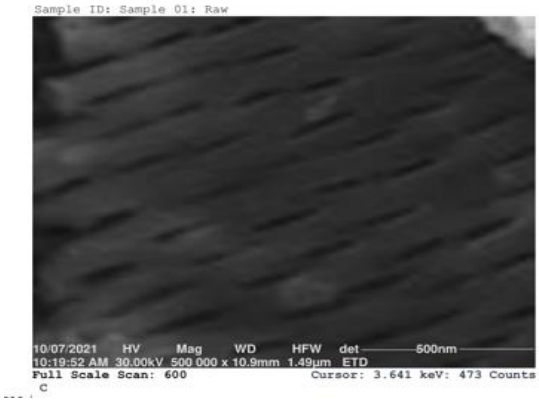

Figure 1 SEM image of the raw FP sample

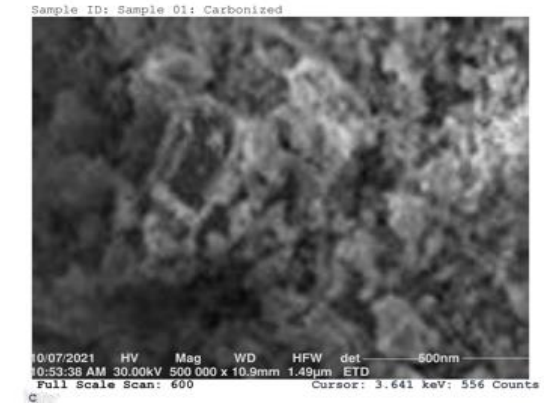

Figure 2 SEM images of the FPAC sample

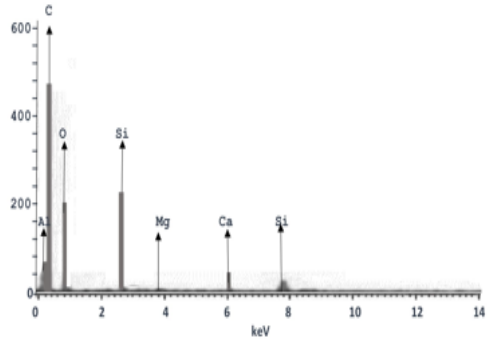

Figure 3 EDX of the raw FP sample

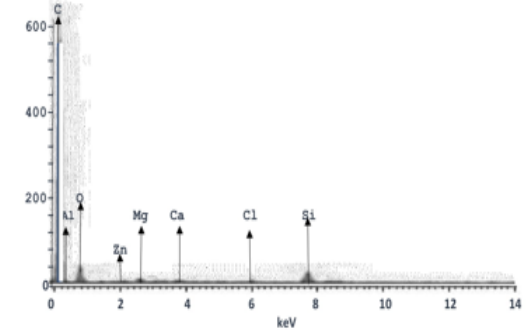

Figure 4 the EDX of the FPAC sample

2.7.3 Surface coverage versus the hopping number

The Hopping number and the surface coverage is expressed in Equation 2.9 while the relationship between the θ versus n is expressed in Equation 2.10 (Anıagor and Menkıtı, 2020)

$$\theta = (1 - \frac{Ce}{Co}) \quad (2.9)$$

$$n = \frac{1}{(1-\theta)\theta} \quad (2.10)$$

2.7.4 Activation energy and sorption probability

The activation energy and the sorption probability, E_a and S* respectively, were evaluated from Equations 2.11 and 2.12 based on the plot of ln(1-θ) against $\frac{1}{T}$ where the intercept and slope are lnS^* and $\frac{E_a}{R}$ respectively (Oladimeji et al., 2025).

$$\ln (1-\theta) = \ln S^* + \frac{E_a}{RT} \quad (2.11)$$

$$\ln (\frac{C_o - C_e}{C_o}) = \frac{E_a}{RT}\frac{1}{T} + \ln S^* \quad (2.12)$$

2.7.5 Eyring equations

The thermodynamic properties (ΔH^- and ΔS^-) used in the Eyring equation (Equations 2.13 and 2.14) were explicitly derived from the adsorption kinetics data under equilibrium-controlled conditions. At each temperature (313-333 K), the apparent rate constant was evaluated from the slope and intercept of the plot of $\ln \frac{k}{T}$ versus $\frac{1}{T}$ (Ebelegi, et al., 2020).

$$\ln \frac{k}{T} = (\ln \frac{k_B}{h} + \frac{\Delta S^-}{R}) - \frac{\Delta H^-}{RT} \quad (2.13)$$

$$\ln \frac{k}{T} = -\frac{\Delta H^-}{R}\frac{1}{T} + (\ln \frac{k_B}{h} + \frac{\Delta S^-}{R}) \quad (2.14$$

where k_B is the Boltzmann constant (1.3807 × 10^{-23} J K^{-1}) and h is the Plank constant (6.6261 × 10^{-34} Js) and R is the universal gas constant (8.314 J mol^{-1} K^{-1}).

Table 1 EDX results of both raw sample of FP and FPAC sample

Element	Raw FP (%)	FPAC (%)
Carbon (C)	43.11	60.75
Oxygen (O)	18.26	10.04
Silicon (Si)	22.47	10.45
Aluminum (Al)	6.12	11.23
Calcium (Ca)	5.47	2.09
Magnesium (Mg)	0.82	2.36
Potassium (K)	6.38	ND
Zinc (Zn)	ND	1.23
Chloride (Cl)	ND	0.95

ND- Not Detected

Table 2 FTIR spectra of raw sample of FP results of analysis

Peak (cm^{-1})	Trans (%)	Bond type	Functional group
3450.29	32.61	O-H	Hydroxyl
2925.43	64.00	CH_2	Alkanes
1750.55	55.72	C=O	CAE
1608.50	64.38	C=C	BR
1429.03	67.21	C-H	AH
1360.96	61.80	C-O	Aldehyde
1250.40	32.05	C-O	Ether
1098.27	44.00	C-O	Alcohols
1025.01	64.26	C-O	Aldehyde
897.63	74.00	C-H	Cellulose

Table 3 FTIR spectra analysis of the FPAC sample

Peak (cm^{-1})	Trans (%)	Bond type	Functional group
3500.01	33.70	O-H	Hydroxyl
2973.17	64.00	C-H	Alkanes
1750.55	53.81	C=O	Carbonyl
1618.37	65.98	N-H	Amine
1497.21	68.09	C-O	AH
1360.98	64.72	C-O	Aldehyde
1250.49	33.51	C-O-C	Ether
1025.01	44.18	C–O	Aldehyde
900.15	65.22	C–H	Alkenes
850.70	70.30	C–H	Alkanes

CAE- Carbonyl, Alkenes and Ester; CA- Carbonyl and Alkenes; AH- Aromatic Hydrocarbon, BR- Benzene ring, Trans- Transmittance.

3. RESULTS AND DISCUSSION

3.1 Development of Activated Carbon from Flamboyant Pod

Flamboyant pod activated carbon was successfully synthesized through KOH activation and carbonization at 500 °C. The activation process promoted pore formation by degrading cellulose, hemicellulose, and lignin components, thus increasing interstitial spacing within the biomass. The breakdown of lignocellulosic structures during activation created a highly porous structure, which is desirable for adsorption. KOH acts as a dehydrating agent, enhancing carbonization and releasing volatiles, which contributes to pore development and surface functionality. This explains why FPAC shows superior adsorption performance compared to raw FP. These structural modifications are consistent with earlier reports (Ravichandran et al., 2018; Nomngongo and Chaba, 2019; Deyi et al., 2023).

3.2 Characterization of FPAC

SEM image (Figure 1) showed that raw FP exhibited dense, rod-like structures, while FPAC displayed porous and dispersed morphologies, confirming the development of adsorption sites shown in Figure 2. EDX analysis revealed elemental compositions dominated by C, O, Si, Al, and Ca (Table 1). In the FPAC sample, potassium disappeared, while Zinc and Chlorine appeared (Figures 3 and 4). Increased carbon content in FPAC suggests enhanced adsorption potential. The increased porosity after KOH activation results from the removal of volatile components and the etching effect of KOH, which widens and develops pores. The disappearance of potassium confirms effective washing, while the higher carbon percentage indicates greater adsorptive potential. The appearance of Zn and Cl may be due to contamination during treatment or enhanced mineral retention in the activated material.

FTIR spectroscopy was employed to identify the surface functional groups present on the raw FP and the KOH-activated FPAC and to evaluate chemical changes induced by alkaline activation. The spectra of raw FP and FPAC are presented in Figures 5 and

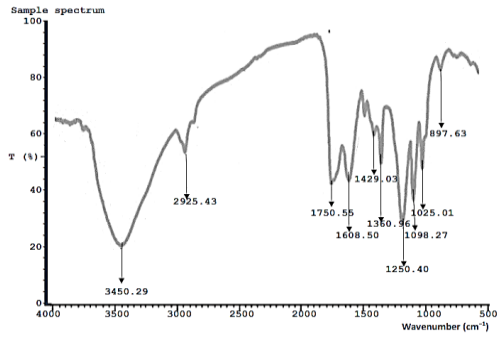

Figure 5 FTIR spectra of the raw sample of FP

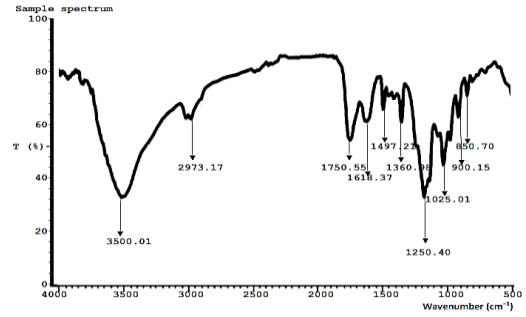

Figure 6 FTIR spectra of the FPAC sample

6, respectively, while the corresponding peak assignments are summarized in Tables 2 and 3.

The FTIR spectrum of raw FP exhibits several characteristic absorption bands associated with lignocellulosic biomass. A broad and intense band at 3450.29 cm^{-1} is attributed to O-H stretching vibrations of hydroxyl groups, arising from cellulose, hemicellulose, lignin, and adsorbed moisture. The peak at 2925.43 cm^{-1} corresponds to aliphatic C-H stretching of $-CH_2$ and $-CH_3$ groups, typical of polysaccharide and lignin structures.

A strong absorption band at 1750.55 cm^{-1} is assigned to C=O stretching vibrations, characteristic of carbonyl groups such as esters, aldehydes, and carboxylic acids presents in hemicellulose and lignin. The band observed at 1608.50 cm^{-1} is assigned to aromatic C=C stretching, confirming the presence of aromatic rings associated with lignin. Peaks in the range 1429.03-1360.96 cm^{-1} are attributed to C-H bending and C-O stretching, associated with aromatic hydrocarbons and aldehyde-type functional groups.

The absorption band at 1250.40 cm^{-1}, is assigned to C-O stretching vibrations, typically arising from ethers, esters, or phenolic groups. Additional peaks at 1098.27 cm^{-1} and 1025.01 cm^{-1} correspond to C-O stretching of alcohols and aldehydes, while the band at 897.63 cm^{-1} is associated with β-glycosidic linkages, confirming the presence of cellulose.

Significant changes in the FTIR spectrum were observed after KOH activation, indicating chemical modification of the FP surface. The broad O-H stretching band persisted at 3500.01 cm^{-1}, though with reduced intensity, suggesting partial dehydration and restructuring of hydroxyl groups during activation. The aliphatic C-H stretching band at 2973.17 cm^{-1} also decreased in intensity, reflecting degradation of aliphatic chains.

The prominent peak at 1750.55 cm^{-1} in FPAC is assigned to C=O stretching, indicating the formation or retention of carbonyl-containing surface groups such as lactones, carboxylic acids, or esters following KOH activation. The appearance of a new band at 1618.37 cm^{-1} is attributed to N-H bending vibrations, suggesting nitrogen incorporation or surface amine functionalities, which can enhance adsorption via hydrogen bonding.

Bands observed at 1497.21 cm^{-1} and 1360.98 cm^{-1} correspond to C-O stretching and C-H bending, associated with aromatic and oxygenated functional groups. The absorption peak at 1250.49 cm^{-1} is assigned to C-O-C stretching vibrations, indicative of ether or ester linkages formed during chemical activation. Additional peaks between 1025.01 and 900.15 cm^{-1} are associated with C-O stretching and aromatic C-H vibrations, while the band at 850.70 cm^{-1} corresponds to out-of-plane C-H bending of aromatic structures.

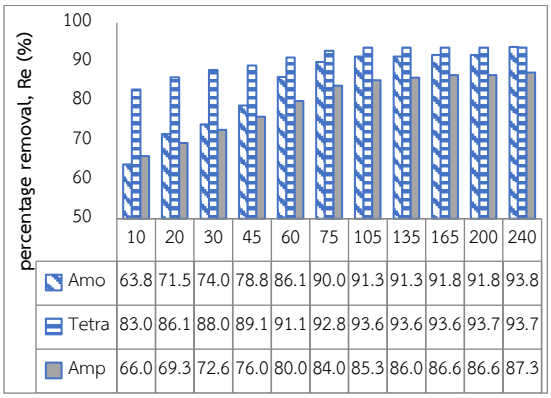

	10	20	30	45	60	75	105	135	165	200	240
Amo	63.8	71.5	74.0	78.8	86.1	90.0	91.3	91.3	91.8	91.8	93.8
Tetra	83.0	86.1	88.0	89.1	91.1	92.8	93.6	93.6	93.6	93.7	93.7
Amp	66.0	69.3	72.6	76.0	80.0	84.0	85.3	86.0	86.6	86.6	87.3

Figure 7 Removal efficiency against effect of contact time

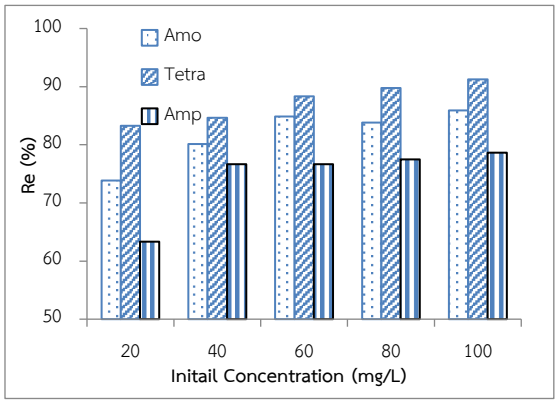

Figure 8 Removal efficiency against initial concentration

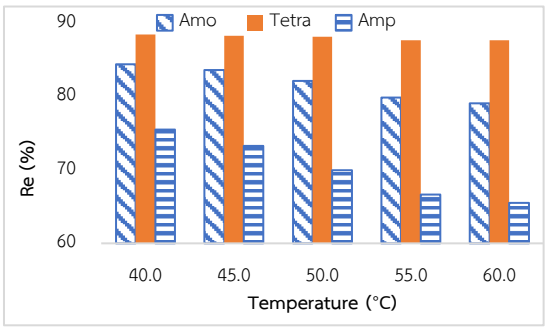

Figure 9 The plot of removal efficiency against temperature

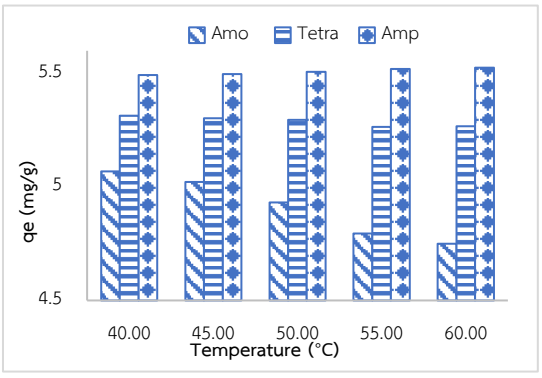

Figure 10 The plot of adsorption capacity against temperature

The emergence and intensification of oxygen-containing functional groups (-OH, -C=O, -C-O-C) and nitrogen-containing groups after KOH activation confirm successful surface modification of FP. These functional groups enhance the affinity of FPAC toward polar antibiotic molecules through hydrogen bonding, **π-π** interactions, and electrostatic attraction, thereby improving adsorption efficiency. The FTIR results are consistent with earlier reports on chemically activated biomass-derived carbons and support the superior adsorption performance of FPAC (Seshadri et al., 2012; Ding et al., 2024).

3.3 Batch Adsorption Studies

The software generated 30 experimental runs that serve as test runs to determine the optimal condition to develop the FPAC that can give high removal efficiency of the selected antibiotics from aqueous solution. Correlation Coefficient (R^2) and standard deviation were used to evaluate the fitness of the model developed. The closeness of R^2 to unity, the smaller the standard of deviation and reasonable agreement between predicted R^2 and adjusted R^2 of less than 0.2, the better the model in predicting the response

Adsorption capacity increased rapidly during the first 100 min, followed by equilibrium plateauing (Figure 7). Maximum adsorption capacities at 100 mg/L were 9.371 mg/g (AMO), 9.310 mg/g (TETRA), and 8.733 mg/g (AMP). TETRA exhibited the highest affinity, followed by AMO and AMP consistent with earlier reports (Sahoo et al., 2018; Wang et al., 2023). The rapid uptake during the initial phase is due to abundant vacant active sites on FPAC. As equilibrium is approached, available sites become occupied, reducing adsorption rate. Higher affinity of TETRA suggests stronger interaction with FPAC functional groups compared to AMO and AMP, possibly due to its larger molecular structure and multiple binding sites.

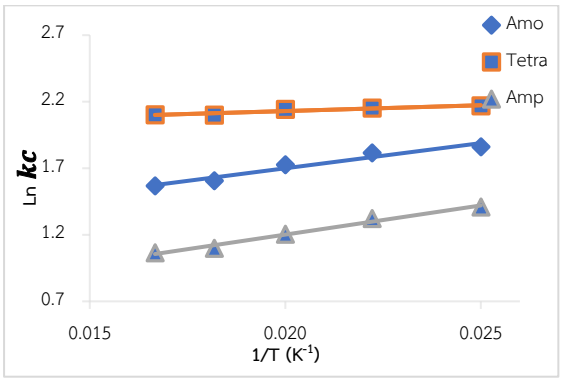

Figure 11 The plots of ln k_c against $\frac{1}{T}$

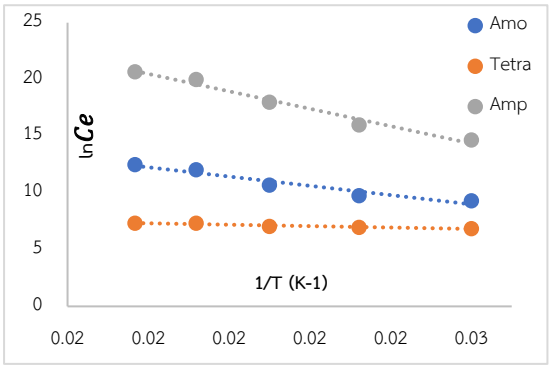

Figure 12 The plots of ln Ce against $\frac{1}{T}$

3.3.1 Effect of contact time and initial concentration

The observed trend confirms that an increase in initial concentration enhances the a capacity of the FPAC. The data presented in Figures 7 and 8 demonstrate that the actual quantity of TAM adsorbed per unit mass of FPAC increased with increasing initial concentration. This behavior can be attributed to the availability of active adsorption sites on the carbon surface. The maximum removal efficiencies were 85.91% (AMO), 91.24% (TETRA), and 78.67% (AMP). These findings agree with Bello et al. (2012) and Deyi et al. (2023), confirming that FPAC offers effective adsorption even at elevated concentrations. At higher initial concentrations, the driving force for mass transfer increases, leading to higher adsorption capacity. This trend reflects competition among TAM molecules for limited adsorption sites.

3.3.2 Effect of temperature

Adsorption decreased with temperature (Figures 9 and 10), with optimum performance at 40 °C, confirming an exothermic adsorption process. At higher temperatures, increased kinetic energy favored desorption, reducing adsorption efficiency. The reduction in adsorption at elevated temperatures indicates an exothermic process. Higher thermal energy disrupts TAM-FPAC bonds, leading to desorption. This suggests that physical forces (e.g., van der Waals interactions, hydrogen bonding) dominate the process (Marczewski et al., 2016; Edet and Ifelebuegu, 2020).

3.4 Thermodynamics Studies

The influence of temperature on the adsorption of selected TAM was examined within the range of 40-60 °C under optimized conditions to evaluate the thermodynamic characteristics of the adsorption process. The findings revealed that the removal efficiency of TAM decreased with increasing temperature, particularly from 40 °C to 55 °C, indicating a temperature-sensitive adsorption process.

3.4.1 Gibbs Free Energy (ΔG°), Enthalpy (ΔH°), and Entropy (ΔS°)

Negative ΔG° values at all tested temperatures confirmed spontaneity and feasibility. The negative enthalpy changes (ΔH° = −31.430, −72.740, and −36.412 kJ·mol^{-1} for AMO, TETRA, and AMP, respectively) (Figure 11) confirm the exothermic nature of adsorption. The high magnitudes of these values indicate that the adsorption process was predominantly physisorption-driven, involving strong specific interactions between the adsorbates and the FP-based adsorbent. Any chemisorption contribution present (-72.740) is secondary and occurs concurrently with physisorption. Positive ΔS° values (7.85, 16.25, 2.71 kJ/mol·K) suggested

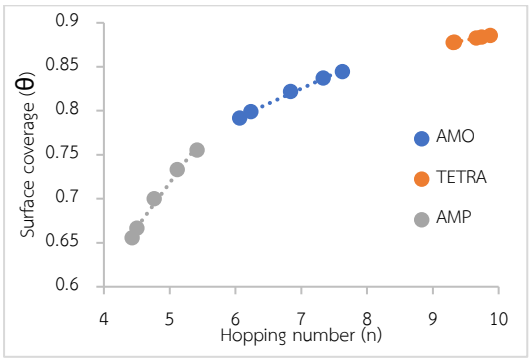

Figure 13: Surface coverage versus hopping number

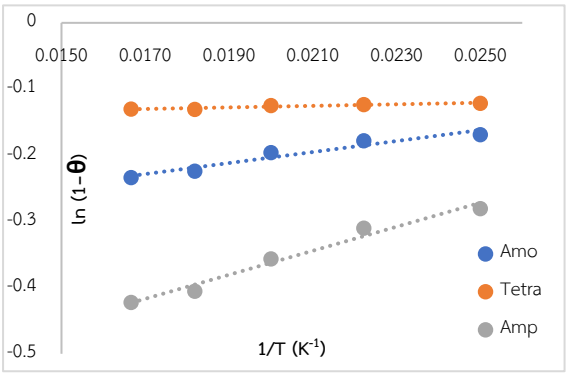

Figure 14 The plot of ln (1−θ) against 1/T

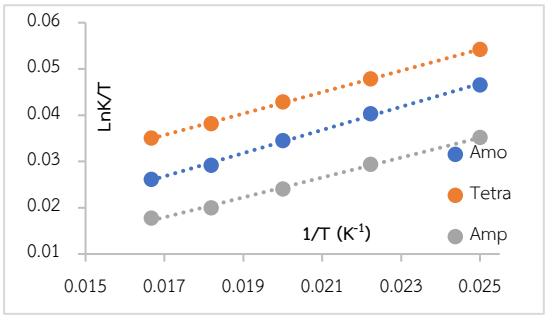

Figure 15 The plot of ln $\frac{k}{T}$ versus $\frac{1}{T}$

increased disorder at the adsorbent-solution interface (Table 4). These results align with similar studies (Xu et al., 2021; Lima et al., 2022). Negative ΔG° confirms feasibility, while negative ΔH° indicates adsorption is energy-releasing. The positive ΔS° suggests randomness increases at the solid-solution interface, likely due to displacement of water molecules and redistribution of solute species upon adsorption.

3.4.2 Isosteric Heat of Adsorption

The Isosteric Heat of Adsorption (ΔH_x) was derived from the slope of the ln C_e versus $\frac{1}{T}$ plot, which displayed linearity across the tested temperature range (Figure 12). The corresponding R^2 and ΔH_x values are presented in Table 5. According to the literature (Neimark *et al.,* 2017; Al-Asadi et al., 2023; Patil et al. 2024), physical adsorption is characterized by ΔH_x values below 40 kJ/mol, while chemical adsorption typically falls within the range of 40-800 kJ/mol. In the present study, the ΔH_x values were 33.94, 51.68, and 63.76 kJ/mol for AMO, TETRA, and AMP, respectively, indicating a predominantly chemical adsorption mechanism. These values also reflect a degree of surface energetic heterogeneity of the FP-activated carbon.

3.4.3 Surface Coverage and Hopping Number

The relationship between surface coverage and hopping number is illustrated in Figure 13. An increase in surface coverage corresponded with an increase in the mobility of the TAM toward vacant binding sites on the adsorbent surface. Variations in surface coverage and hopping number among AMO, TETRA, and AMP indicate that ampicillin more readily located binding sites on the adsorbent. The hopping number, which reflects the rate of molecular migration to adsorption sites, was smallest for AMP, suggesting a faster adsorption process. These observations are consistent with previous findings reported by Menkiti et al. (2014) and Anıagor and Menkıtı, (2020).

3.4.4 Activation Energy and Sticking Probability

Activation energy (E_a) values were calculated from the slope of the appropriate Arrhenius plot (Figure 14) and found to be 6.9088, 9.7706, and 15.0842 kJ/mol for AMO, TETRA, and AMP, respectively. As presented in Table 5, the sticking probability (S*) values for all antibiotics ranged between 0 and 1, confirming a favorable adsorption process characterized by a high likelihood of TAM

Table 4 Thermodynamic parameters for the uptake of AMO, TETRA and AMP onto FPAC

Adsorbate / Parameters	Tempt. (K)	Amo	Tetra	Amp
R^2		0.9539	0.8924	0.9845
ΔH (kJ/mol)		-31.430	-72.740	-36.412
ΔS (kJ/gmol K)		7.8459	16.25	2.7079
ΔG (kJ/mol)	313.0	-2.7701	-5.1597	-1.2117
ΔG (kJ/mol)	318.0	-2.8093	-5.2409	-1.2252
ΔG (kJ/mol)	323.0	-2.8485	-5.3222	-1.2388
ΔG (kJ/mol)	328.0	-2.8878	-5.4035	-1.2523
ΔG (kJ/mol)	333.0	-2.9270	-5.4847	-1.2659

Table 5 Isosteric heat of adsorption, sticking probability and activation energy parameters

Adsorbate / Parameters	Amo	Tetra	Amp
$\triangle H_x$ (KJ/mol)	33.94	51.68	63.76
K	19.20	8.38	33.52
R^2	0.9429	0.8883	0.9790
E_a (kg/mol)	6.9088	9.7706	15.0842
S^*	0.6909	0.8606	0.4842

Table 6 Antibiotic uptake of Eyring equations parameters

Adsorbate / Parameters	Tempt (K)	Amo	Tetra	Amp
R^2		0.9975	0.9995	0.9966
ΔH^- (kJ/mol)		-20.832	-19.261	-17.869
ΔS^- (kJ/mol)		-1.97370	-1.97270	-1.9739
ΔG^- (kJ/mol)	313	61.7560	61.7262	61.7652
ΔG^- (kJ/mol)	318	62.7428	62.7126	62.7522
ΔG^- (kJ/mol)	323	63.7297	63.6990	63.7391
ΔG^- (kJ/mol)	328	64.7165	64.6853	64.7261
ΔG^- (kJ/mol)	333	65.7034	65.6717	65.7130

molecules adhering to the FP surface. These S* values indicate that the adsorption mechanism is primarily dependent on the adsorbate, adsorbent system and the temperature of the process (Ebelegi et al., 2020).

The positive values of E_a simply indicates the presence of an energy barrier that must be overcome before adsorption occurs. And the relatively low E_a values further indicate that the adsorption process is dominated by physisorption and is diffusion-assisted, requiring only a small energy barrier for adsorbate-adsorbent interaction. The positive E_a values confirm the presence of an activation barrier, while the exothermic nature of the process is evidenced by the negative ΔH° values. Similar observations have been reported for biomass-derived adsorbents (Echereme et al., 2019; Ebelegi et al., 2020).

3.4.5 Eyring equations

Thermodynamic evaluation using the Eyring equation yielded large positive ΔG^- values, indicating that a significant amount of energy is required to activate the adsorption process. Thus, the reported ΔG^- values (61.76-65.71 kJ/mol across 313-333 K) as shown in Figure 15, directly reflect the temperature-dependent rate constants governing the adsorption process.

The negative ΔH^- values for AMO (−20.83 kJ/mol), TETRA (-19.26 kJ/mol), and AMP (-17.87 kJ/mol) confirm the formation of the activated complex is exothermic nature of the adsorption. Furthermore, the negative entropy changes, -1.9737, -1.9727, and -1.9739 kJ/mol·K, respectively, as shown in Table 6, suggests an associative transition state characterized by increased ordering as antibiotic molecules interact with the FPAC surface. This ordering is consistent with surface-controlled adsorption rather than bulk diffusion.

The positive ΔG^- values observed at all temperatures confirm the presence of an energy barrier that must be overcome for adsorption to proceed, indicating that although the process is thermodynamically favorable overall, it is kinetically controlled. These observations are consistent with previous adsorption studies employing the Eyring formalism (Ebelegi et al., 2020; Mechnou et al., 2022).

4. CONCLUSION

This study demonstrated that Flamboyant-pod-based activated carbon is an efficient, low-cost, and environmentally friendly adsorbent for the removal of a ternary antibiotic mixture (amoxicillin, tetracycline, and ampicillin) from aqueous solutions. Batch adsorption studies revealed that adsorption efficiency was influenced by concentration, contact time, and temperature, with optimum adsorption observed at 40 °C. Characterization by SEM, EDX, and FTIR confirmed significant surface modifications and pore development following KOH activation and carbonization. Thermodynamic analysis revealed negative $\Delta G°$ and $\Delta H°$ values, confirming that the process was spontaneous and exothermic. The isosteric heat of adsorption and activation energy values suggested that the adsorption was primarily physisorption-controlled. FPAC shows significant promise as a sustainable and effective adsorbent for the remediation of antibiotic-contaminated wastewater, contributing to environmental pollution control and resource valorization of agricultural residues.

REFERENCES

Abdelkarim, S., & Djamila, H. (2020). Wastewater management challenges and solutions. *Journal of Environmental Science and Health, 55*(4), 320-330.

Abulude, F. O., & Adejayan, A. O. (2017). Agricultural residues as low-cost adsorbents for wastewater treatment. *Applied Water Science, 7*(6), 3651-3661.

Al-Asadi, S. T., Al-Qaim, F. F., Al-Saedi, H. F. S., Deyab, I. F., Kamyab, H., & Chelliapan, S. (2023). Adsorption of methylene blue dye from aqueous solution using low-cost adsorbent: kinetic, isotherm adsorption, and thermodynamic studies. *Environmental Monitoring and Assessment*, *195*(6), 676. doi: 10.1007/s10661-023-11334-2.

Alnajrani, M. N., & Alsager, O. A. (2020). Antibiotics in wastewater: Occurrence, fate, and removal technologies. *Science of the Total Environment, 720*, 137574. https://doi.org/10.1038/s41598-020-57616-4

Amrutha, J. G., Girish, C. R., Prabhu, B., & Mayer, K. (2023). Multi-component adsorption isotherms: review and modeling studies. *Environmental processes*, *10*(2), 38-52 https://doi.org/10.1007/s40710-023-00631-0

Anıagor, C. O., & Menkıtı, M. C. (2020). Relational description of an adsorption system based on isotherm, adsorption density, adsorption potential, hopping number and surface coverage. *Sigma Journal of Engineering and Natural Sciences*, *38*(3), 1073-1098.

Azarpira, H., Mahdavi, M., & Nazari, R. (2019). Removal of pharmaceuticals from water using adsorption: A review. *Journal of Cleaner Production, 223*, 122-139.

Barbooti, M. M., & Zahraw, Z. J. (2020). Antibiotics in wastewater: Impacts and challenges. *Environmental Processes, 7*(2), 459-472.

Bello, O. S., Adegoke, K. A., & Olaniyan, A. A. (2012). Adsorptive removal of pharmaceuticals from aqueous solutions. *Desalination and Water Treatment, 44*(1–3), 1-10.

Choffor-Nchinda, E., Atanga, L. C., Nansseu, J. R., & Djomou, F. (2018). Effectiveness of amoxicillin alone in the treatment of uncomplicated acute otitis media: a systematic review protocol. *BMJ open*, *8*(6), e021133.

Deyi, A. V., Yaumi, A. L., Umar, H., Aji, M. M., & Mustafa, B. G. (2023). Adsorptive properties of Flamboyant seed pod activated carbon for the removal of anionic dye in wastewater. *Arid Zone Journal of Basic and Applied Research, 2* (5), 124-131.

Ding, J., Liang, J., Wang, Q., Tan, X., Xie, W., Chen, C., & Chen, X. (2024). Enhanced tetracycline adsorption using KOH-modified biochar derived from waste activated sludge in aqueous solutions. *Toxics*, *12*(10), 69-81.

Dufatanye, I., Lee, Y., Kim, H., & Lee, S. (2022). Industrial wastewater discharge and compliance investigation for environmentally resilient Rwanda. *Water*, *14*(19), 3100. https://doi.org/10.3390/w14193100

Ebelegi, A. N., Ayawei, N., & Wankasi, D. (2020). Interpretation of adsorption thermodynamics and kinetics. *Open Journal of Physical Chemistry*, *10*(3), 166-182. https://doi.org/10.4236/ojpc.2020.103010

Echereme, C. B., Nworie, O. E., & Edeh, I. J. (2019). Adsorption of pollutants on porous adsorbents at elevated temperatures. *Environmental Technology, 40*(15), 2021-2033.

Edet, U. A., & Ifelebuegu, A. O. (2020). Kinetics, Isotherms, and Thermodynamic Modeling of the Adsorption of Phosphates from Model Wastewater Using Recycled Brick Waste. *Processes*, *8*(6), 665. https://doi.org/10.3390/pr8060665

Fomnya, H. J., Ngulde, S. I., Amshi, K. A., & Bilbonga, G. (2021). Antibiotics: Classifications and mechanism of resistance. *International Journal of Applied Microbiology and Biotechnology Research, 9*(15), 38-50.

Gautam, R., Priyadarshini, E., Patel, A. K., & Arora, T. (2024). Assessing the impact and mechanisms of environmental pollutants (heavy metals and pesticides) on the male reproductive system: a comprehensive review. *Journal of Environmental Science and Health, Part C*, *42*(2), 126-153.

George, A., Brown, R., & Wilson, D. (2014). Analytical methods in FTIR spectroscopy for biomass characterization. *Spectrochimica Acta Part A: Molecular and Biomolecular Spectroscopy, 133*, 200-208.

Hasan, M. N., Rahman, M., & Alam, A. (2014). Effect of temperature on adsorption of pharmaceuticals. *Journal of Environmental Management, 143*, 145-152.

Korkmaz, Ş., & Tuna, Ö. Adsorption potential of spherical ZnO particles for sufficient antibiotic removal: isotherm, kinetic and thermodynamics. *Journal of Innovative Engineering and Natural Science*, *5*(1), 19-29.

Lima, E. C., Hosseini-Bandegharaei, A., Moreno-Piraján, J. C., & Anastopoulos, I. (2019). A critical review of the estimation of the thermodynamic parameters on adsorption equilibria. Wrong use of equilibrium constant in the Van't Hoof equation for calculation of thermodynamic parameters of adsorption. *Journal of molecular liquids*, *273*, 425-434. https://doi.org/10.1016/j.molliq.2018.10.048

Marczewski, A. W., Deryło-Marczewska, A., & Jaroniec, M. (2016). Influence of temperature on adsorption capacity of antibiotics. *Applied Surface Science, 362*, 560-570.

Mashkovtsev, M., Tarasova, N., Baksheev, E., Rychkov, V., Zhuravlev, N., Solodovnikova, P., & Galiaskarova, M. (2023). Spectroscopic Study of Five-Coordinated Thermal Treated Alumina Formation: FTIR and NMR Applying. *International Journal of Molecular Sciences*, *24*(6), 5151. https://doi.org/10.3390/ijms24065151.

Mechnou, I., Meskini, S., El Ayar, D., Lebrun, L., & Hlaibi, M. (2022). Olive mill wastewater from a liquid biological waste to a carbon/oxocalcium composite for selective and efficient removal of methylene blue and paracetamol from aqueous solution. *Bioresource technology*, *365*, 128162. https://doi.org/10.1016/j.biortech.2022.128162

Nafisur, R., & Poornima, V. (2020). Assessment of ampicillin removal efficiency from aqueous solution by polydopamine/zirconium (IV) iodate: optimization by response surface methodology. *The Royal Society of Chemistry, 10*(34), 322–337.

Neimark, A. V., Tarazona, P., & Seaton, N. A. (2017). Thermodynamics of adsorption and isosteric heat evaluation. *Colloids and Surfaces A: Physicochemical and Engineering Aspects, 529*, 23-33.

Nomngongo, P. N., & Chaba, R. (2019). KOH-activated carbons for wastewater treatment. *Journal of Environmental Science and Health, Part A, 54*(5), 441-452.

Okoye, C. O., Okoye, P. U., & Obi, C. (2018). Calibration and adsorption study of antibiotics in aqueous solution. *Journal of Environmental Chemical Engineering, 6*(2), 1531-1540.

Oladimeji, F. O., Alade, A. O., Tijani, I. O., Abdulrasheed, W. A., Olarinde, M. O., Ilori, K. P., & Afolabi, T. J. (2025). Thermodynamic Properties of Polyaromatic Hydrocarbons Adsorption from Wastewater using Pineapple-Crown-Based Cellulose. *International Journal of Academic Engineering Research (IJAER) 9*(3), 80-87.

Ortúzar, M., Esterhuizen, M., Olicón-Hernández, D. R., González-López, J., & Aranda, E. (2022). Pharmaceutical pollution in aquatic environments: a concise review of environmental impacts and bioremediation systems. *Frontiers in microbiology*, *13*, 869332. https://doi.org/10.3389/fmicb.2022.869332

Patil, P., Jeppu, G., Vallabha, M. S., & Girish, C. R. (2024). Enhanced adsorption of phenolic compounds using biomass-derived high surface area activated carbon: Isotherms, kinetics and thermodynamics. *Environmental Science and Pollution Research*, *31*(60), 67442-67460.

Rahmanian, B., Ali, A., & Bukhari, A. (2018). Effect of concentration on antibiotic adsorption. *Environmental Technology and Innovation, 9*, 110-119.

Ravichandran, P., Kumar, R., & Raj, R. (2018). KOH activation and carbonization of agricultural residues. *Carbon Resources Conversion, 1*(3), 233-241.

Renugadevi, K., & Krishnaveni, R. (2021). Comparative evaluation of wastewater treatment methods. *Journal of Water Process Engineering, 40*, 101967.

Roberts, M., & Chopra, I. (2021). Tetracycline Antibiotics: Mode of Action, Applications, Molecular Biology, and Epidemiology of Bacterial Resistance. *American Society for Microbiology, 65*(2), 232-260.

Sahoo, P. K., Patel, R. K., & Ray, S. K. (2018). Adsorption kinetics and thermodynamics of tetracycline on activated carbon. *Applied Surface Science, 427*, 513-523.

Sarwar, A., Ali, M., Khoja, A. H., Nawar, A., Waqas, A., Liaquat, R., & Asjid, M. (2021). Synthesis and characterization of biomass-derived surface-modified activated carbon for enhanced CO2 adsorption. *Journal of CO2 Utilization*, *46*, 101476. https://doi.org/10.1016/J.JCOU.2021.101476

Seshadri, V., Singh, K., & Mehta, M. (2012). FTIR analysis of chemically modified biomass. *Spectroscopy Letters, 45*(3), 214-222.

Wang, C., Feng, X., Shang, S., Liu, H., Song, Z., & Zhang, H. (2023). Adsorption of methyl orange from aqueous solution with lignin-modified metal–organic frameworks: Selective adsorption and high adsorption capacity. *Bioresource Technology*, *388*, 129781. https://doi.org/10.1016/j.biortech.2023.129781

Wei, J., Li, X., & Zhang, Y. (2019). Adsorption of antibiotics in multicomponent systems. *Journal of Hazardous Materials, 368*, 685-693.

Xu, H., Wang, J., & Liu, S. (2021). Thermodynamic insights into antibiotic adsorption. *Chemical Engineering Journal, 420*, 129646.

Zeng, F., Chen, H., Mei, Y., Ye, L., Zhuang, S., Pu, N., & Wang, L. (2024). Performance and mechanism of sulfonamide-antibiotic adsorption by Ti3 C2 MXene. *New Journal of Chemistry, 48(38)*, 16742-16752.